npj | materials degradation

Article

Published in partnership with CSCP and USTB

https://doi.org/10.1038/s41529-024-00452-y

Enhancement resistance to microbiologically influenced stress corrosion of Cu-bearing steel against *Bacillus cereus*

Bo Liu [1,2], Fangyuan Lu[3], Shidong Zhu[1,2], Cuiwei Du [3,4,5] ✉ & Xiaogang Li[3,4,5]

Microorganisms are notoriously known to cause local corrosion and stress corrosion cracking (SCC), which seriously endangers the materials service safety. Cu can enhance antibacterial function of the material and reduce the vulnerability to hydrogen embrittlement (HE). However, the dilemma of how much Cu content generates the best resistance to microbiological corrosion and SCC arises. Here, we modified the Cu content in pipeline steel to obtain the best antibacterial effect to nitrate reducing bacteria *Bacillus cereus* and HE resistance. The findings offer a fresh perspective on how to design and prepare a steel that are both resistant to microbiological corrosion and SCC.

Research on microbiologically influenced corrosion (MIC) is becoming an important cross-discipline in the field of corrosion, and the MIC mechanism has been gradually uncovered[1,2]. This includes not only the influence of extracellular electron transfer, but also the mechanisms that directly or indirectly affect corrosion, such as cathode depolarization, secretion of organic acids and biological cathode catalysis[3–6]. MIC occurs commonly in oil well casing, long-distance pipeline and underwater pipeline, and is one of the most challenging problems to handle in industrial corrosion[7,8]. MIC can generate local corrosion or pitting on the metal surface, which will lead to the occurrence of stress corrosion cracking (SCC) under the impact of external pressures[9,10]. It is thought that sulfate reducing bacteria (SRB) activity will speed crack initiation and growth, create secondary corrosion at the pit bottom, and cause ductile fractures to become brittle fractures[11,12]. SRB encourages hydrogen penetration and pitting development, particularly at cathode potential, which enhances the sensitivity to SCC[13,14]. Recently, numerous research on the MIC of nitrate-reducing bacteria (NRB) have been conducted. Anaerobic respiration allows NRB to get electrons from the steel matrix, which is thermodynamically more advantageous than SRB[15,16], and the nitrite, the reduction product of NRB, can also accelerate corrosion[17–19]. Further, NRB can accelerate the cathode hydrogen evolution reaction through hydrogen depolarization, which can also promote the SCC sensitivity of steel[20]. It is clear that these microbes can promote SCC, which is what many researchers are currently focusing on[21,22].

How to alleviate and control the influence of microorganisms on SCC is one of the main goals of investigating MIC. Therefore, it is best to prevent microbes from adhering to and reproducing on material surfaces[23,24]. From the standpoint of the material itself, the direct antibacterial characteristic of metal materials is a crucial way to prevent or lessen SCC[25,26]. The addition of Cu to metal alloys has been established, particularly in Ti alloy, and has a wide range of uses because Cu and Ag are naturally occurring antibacterial components[27]. Cu helps prevent MIC, however maintaining Cu ion release over an extended period of time is a major difficulty that restricts the mechanical capabilities and corrosion resistance of material. Good bacteriostatic effects were observed when 1–3 wt.% Cu was added to 2205 and 304 stainless steel, however the impact toughness dropped as the Cu concentration increased[28–31]. It has been established in recent years that adding Cu element to gram-negative *P. aeruginosa* and gram-positive *B. vietnamensis* has a greater than 99% antibacterial rate[32,33]. Gram-positive *Bacillus cereus (B. cereus)* has been shown to have a high resistance to Cu, however, the antibacterial impact becomes considerable at concentrations higher than 4 mmol[34]. Similarly, the inhibition rate of gram-positive bacteria for some Cu-doped nanoparticles exceeds 99%[35]. Cu has been frequently utilized to limit microbial corrosion and reproduction because it can impact the roles of bacteria in metal formation, membrane remodeling, and antioxidant activity.

Interestingly, Cu has good antimicrobial qualities as well as a favorable impact on resistance to hydrogen embrittlement (HE)[36,37]. The structure of

[1]School of Materials Science and Engineering, Xi'an Shiyou University, Xi'an 710065, China. [2]Key Laboratory of Corrosion Protection and New materials for Oil and Gas Fields of Shaanxi Higher Education Institutes, Xi'an Shiyou University, Xi'an 710065, China. [3]Institute for Advanced Materials and Technology, University of Science and Technology Beijing, 100083 Beijing, China. [4]Key Laboratory for Corrosion and Protection of the Ministry of Education (MOE), 100083 Beijing, China. [5]National Materials Corrosion and Protection Scientific Data Center, 100083 Beijing, China. ✉e-mail: dcw@ustb.edu.cn

the Cu-rich precipitated in tempered martensitic steel can significantly reduce the HE sensitivity of the steel by up to 55.3%, while keeping the steel the same resistance to limit tensile strength, of which 9R-Cu is the strongest combination with hydrogen and the highest capability[38]. Similarly, the synergistic effect of Cu and austenite on HE in low carbon and low alloy steels shows that the addition of Cu promotes the formation of Cu-rich precipitates, in which the BCC rich Cu-phase with the substrate's conjugate/semi-conjugate phase is the strong capture concentration point of hydrogen, and the weak capture point of FCC rich Cu-phase is the hydrogen dispersed phase[39]. When hydrogen is tightly mixed with these Cu-rich materials, it reduces the amount of diffusible hydrogen, homogenizes the diffused hydrogen, lowers the local hydrogen concentration at the interface, and lessens the material sensitivity to hydrogen embrittlement[40,41]. It is a valuable idea to add Cu to pipeline steel to increase the resistance of MIC and SCC, but the Cu content must also be taken into account to balance the link between its mechanical qualities and HE resistance.

Based on the above understanding and discovery of anticorrosion mechanism, a series of Cu alloying was designed and studied to investigate 1) the effects of pipeline steels with different Cu contents on antibacterial efficacy of *B. cereus*, 2) the effects of different Cu contents on SCC of pipeline steel, and 3) the effects of different Cu contents on antibacterial efficacy of *B. cereus* and SCC. To answer these questions, we used slow strain rate tensile test (SSRT), live/dead staining, and electrochemical techniques to confirm that the findings not only expand the range of uses for Cu-bearing pipeline steel that is resistant to MIC, but also design a steel that are both highly strong and highly resistant to SCC.

Results and discussion

Material characteristics

Table 1 displays the mechanical characteristics of several Cu-bearing steels after aging treatment. The yield strength and tensile strength both significantly rise with an increase in Cu content, particularly when the Cu content is 2.0 wt.% or above, which reaches X100 steel performance (yield strength 690–840 MPa, tensile strength 760–990 MPa). However, the impact toughness of 2.0Cu steel is only 22.2% of 0.0Cu steel, according to additional examination, which means it is not an appropriate alternative material for research.

Table 1 | Mechanical properties of Cu-bearing pipeline steel (error bars stand for the standard deviations from three independent samples)

	Yield strength, MPa	Tensile strength, MPa	Elongation, %	Impact toughness, J
0.0Cu	543 ± 3.5	612 ± 2.6	14.62 ± 0.4	152.9 ± 2.6
0.6Cu	609 ± 4.1	687 ± 1.9	12.76 ± 0.7	171.1 ± 3.3
1.0Cu	629 ± 2.8	751 ± 3.4	12.45 ± 0.8	135.7 ± 1.8
2.0Cu	720 ± 3.3	878 ± 1.7	9.12 ± 0.5	34.0 ± 1.4

Figure 1 shows the microstructure morphologies of different Cu-bearing steels. The three different types of steel have polygonal ferrite and bainite microstructures, and the addition of Cu is conducive to the refinement of grain. The microstructure of 0.6Cu steel and 1.0Cu steel was further selected for TEM analysis, and the results are depicted in Fig. 2. The microstructure of 0.6Cu steel is composed of crisscrossed non-parallel ferrite bars, and no fine nano-precipitates are found in further observation. The composition identification of randomly chosen places reveals that Fe is the predominant element component and that there is not a noticeable Cu peak, indicating that despite the addition of 0.6 wt.% Cu to the steel, the trace composition is insufficient for Cu to be visibly present in the material. For 1.0Cu steel, a significant number of granular precipitates are disseminated at the grain boundary or subboundary, as depicted in Fig. 2d. The particle area (approximately 20 nm in diameter) was selected for component identification, and the result was shown as a noticeable Cu peak, indicating that 1.0Cu steel can be dispersed after 1 h aging treatment for a nanoscale Cu-rich phase.

EIS

Figures 3 and 4 exhibit the Nyquist and Bode diagrams of the impedance measurements for different Cu-bearing steels exposed to abiotic and biotic medium. In abiotic medium, with the passage of immersing time, the three Cu-bearing steels exhibits a relatively complete arc resistance, and its radius slightly decreases with varying immersing times, as can also be determined from the modulus value. These findings suggest that the rate of corrosion of Cu- bearing steel in an oxygen-free environment is not significantly affected over time. However, in biotic medium, the arc radius of the three Cu-bearing steels increases with time, suggesting that their corrosion resistance does as well. At the same time, it is evident that as the Cu content increases, the data of the capacitive reactance arc at the low frequency stage drops, indicating a decrease in the interface reaction and an increase in reaction resistance.

To further explore the evolution of the interfacial reaction, equivalent circuit was employed to model the EIS data, as shown in Fig. 5a. In this circuit, R_s represents the solution resistance, Q_f is the capacitance of the mixed layer of corrosion product and biofilm, R_p is the pore resistance in biotic medium, and Q_{dl} and R_{ct} represent the double layer capacitance and charge transfer resistance, respectively. Figure 5b also displays the law of the $R_{ct} + R_p$ value, which reflects the change of the corrosion rate. In the sterile environment, the $R_p + R_{ct}$ value of 0.0Cu steel remained relatively constant within 14 days, suggesting a consistent rate of corrosion. The R_p+R_{ct} value of 0.6Cu steel increases gradually, indicating that the corrosion rate decreases with the increase of immersing time. The R_p +R_{ct} value of 1.0Cu steel decreased slightly after 7 days, suggesting that the rate of corrosion had accelerated. In the biotic medium, the $R_p + R_{ct}$ values of the three Cu-bearing steels all rose in the presence of *B. cereus*, suggesting a close relationship between the change in *B. cereus* and the rate of corrosion. The values of 0.6Cu and 1.0Cu steel after three days are larger than those of 0.0Cu steel, indicating that the corrosion rate is relatively small at this time, which may be related to the growth of Cu ions on *B. cereus* and the formation of biofilm.

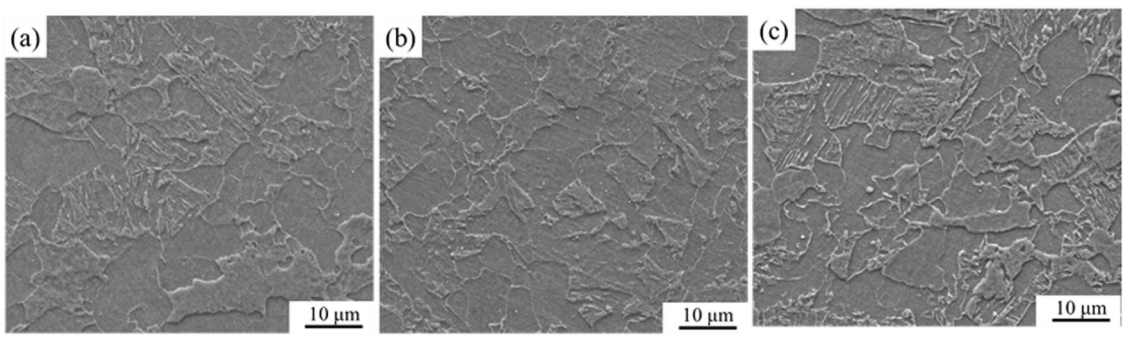

Fig. 1 | Microstructure of steel with different Cu content. a 0.0Cu, **b** 0.6Cu, **c** 1.0Cu.

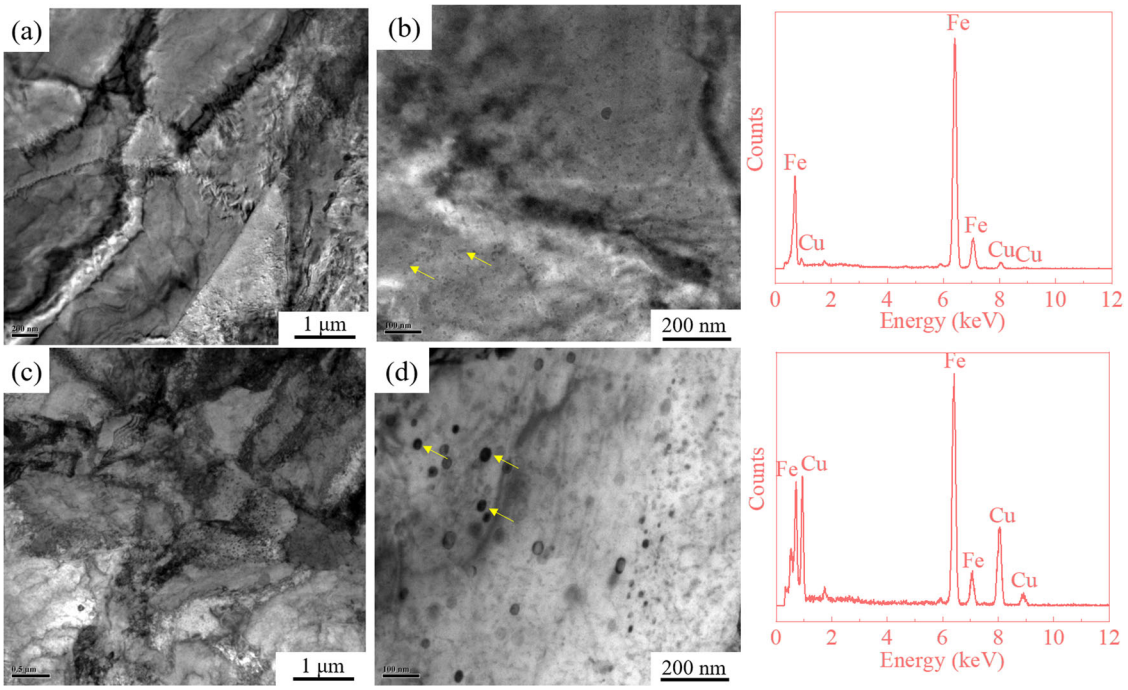

Fig. 2 | TEM results of steels with different Cu content. a, **b** 0.6Cu, **c**, **d** 1.0Cu (The arrow marks are the EDS identification points).

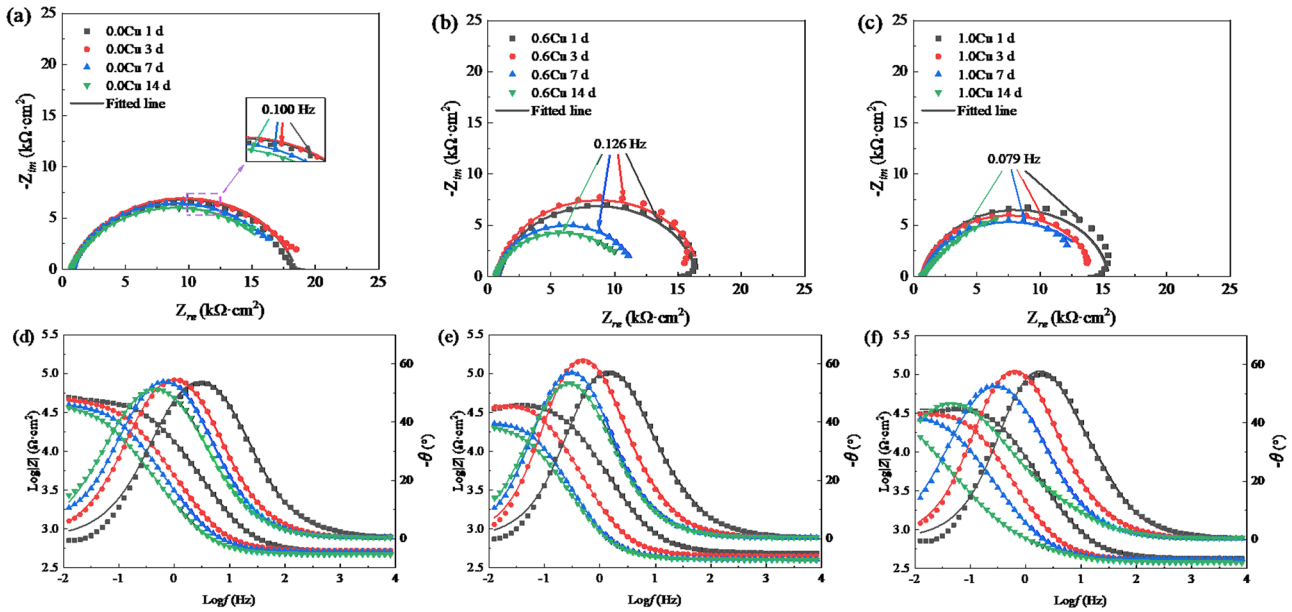

Fig. 3 | EIS results of steel with different Cu content in abiotic medium for different days. a, **d** 0.0Cu, **b**, **e** 0.6Cu, **c**, **f** 1.0Cu.

Surface morphology and composition analysis

According to EIS data, Cu-bearing steel corrodes more quickly in biotic medium than it does in sterile medium. As a result, we solely take into account variations in the various Cu concentrations in the bacterial environment when observing morphology. Figure 6 shows the surface morphology and composition analysis of different Cu-bearing steels after being immersed for 7 days in biotic medium. As can be observed from the surface morphology, biofilm clusters were formed on the surface of the sample, and there was no variation in the morphology of *B. cereus* on the surface of different Cu-bearing steels. The lateral morphology shows the local corrosion of the 0.0Cu steel surface is more pronounced, and the pit depth is about 10 μm. From the distribution of the elements, it is indicated that a large number of P elements are distributed in the product, mainly the components of *B. cereus* and biofilms. The most obvious is that the distribution of Cu content increases with the increase of the design content, indicating that the change in Cu content in steel is the only factor affecting the differences in MIC. Analyzing the composition of the Cu element on the surface of the sample, there is no effective peak found on the 0.0Cu steel surface, and the strength of the peak becomes increasingly apparent with the increase in the Cu content. 0.6Cu steel is composed of CuO (933.4 eV) and Cu_2O (932.8 eV), and 1.0Cu steel is composed of Cu_2O (932.6 eV). CuO and Cu_2O are generated on the steel surface in an oxygen-free environment, primarily as a result of the sample coming into contact with air during dehydration.

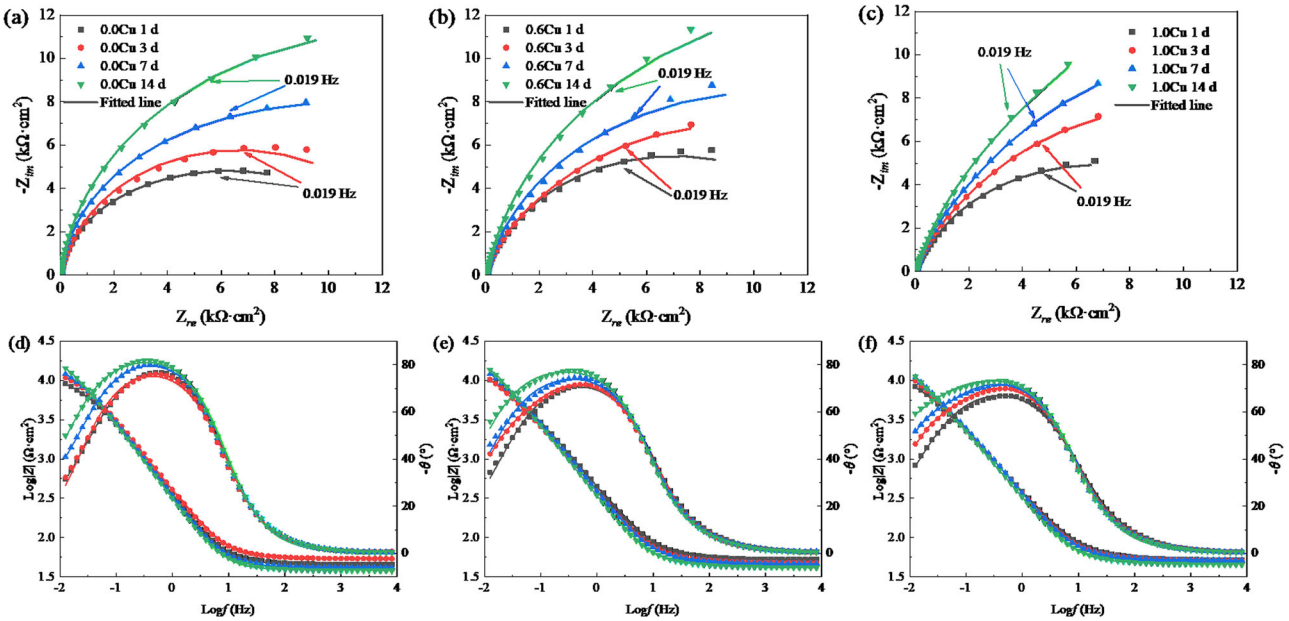

Fig. 4 | EIS results of steel with different Cu content in biotic medium for different days. a, **d** 0.0Cu, **b**, **e** 0.6Cu, **c**, **f** 1.0Cu.

Fig. 5 | Electrical equivalent circuit used for fitting the EIS spectra. a Equivalent circuit, **b** R_{ct}+R_p value (mean ± standard deviation).

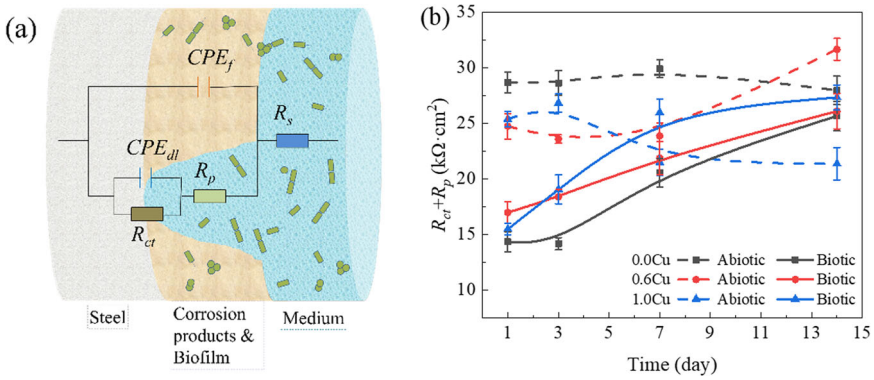

Antibacterial efficacy

The above studies show that the contents of Cu in steel have a clear effect on MIC, and in order to further investigate the effects of Cu content on *B. cereus*, triplicate coupons of each metal were immersed in media containing *B. cereus*. Figures 7 and 8 shows the colony numbers after 1, 3, 7, and 14 days of incubation and the representative samples, respectively. With the passage of immersion time, the number of *B. cereus* increased first and then decreased, which was consistent with its growth cycle. Compared with 0.0Cu steel, 0.6Cu steel and 1.0Cu steel decreased slightly on the 3rd day, and the decrease was more obvious on the 7th day, indicating that the increase of Cu content has a significant effect on the number of live bacteria on the surface of the sample, which means that the Cu-bearing steel has certain antibacterial property.

The viability of *B. cereus* cultured on steel surface for 7 days was evaluated by live/dead staining techniques. Figure 9 shows both green and red bacteria on the surface of 0.0Cu and 0.6Cu, indicating that there are both live bacteria and dead bacteria. Careful observation shows that the number of dead bacteria on 0.6Cu steel is more than that on 0.0Cu steel. There are only a small amount of green bacteria on the surface of 1.0Cu steel, and most of them are red bacteria, indicating that there are a large number of dead bacteria. The above difference fully demonstrates that in the same environment, different Cu content has a certain effect on the number of live/dead bacteria on the surface of steel, and with the increase of Cu content, the ability to poison *B. cereus* becomes stronger.

Stress-strain curves and SCC susceptibility

Figure 10 shows the stress-strain curves and corresponding SCC susceptibility of different Cu-bearing steels at open circuit potential (OCP) and −0.9 V in air, abiotic and biotic media. With the increase of Cu content, the yield strength gradually increases from 543 MPa to 629 MPa, while the elongation decreases from 14.62% to 12.45%, indicating that the increase of Cu content can increase the strength of the material, but also slightly reduce the elongation. The effects of different Cu contents on *B. cereus* and potential were further analyzed by SCC sensitivity indexes. As shown in Fig. 10d, the SCC sensitivity of different Cu-bearing steel in abiotic medium under OCP was 7.54%, 6.89% and 10.66%, while it was 16.15%, 10.78%, 16.38% in biotic medium. The results showed that the SCC susceptibility was the lowest when Cu content was 0.6 wt.%, and increased when Cu content was not added or 1.0 wt.%. Therefore, the SCC sensitivity of *B. cereus* to 0.0Cu, 0.6Cu and 1.0Cu steels at OCP was increased by 8.61%, 3.89% and 5.72%, respectively, indicating that Cu addition can reduce the effect of *B. cereus* on SCC. The sensitivity of SCC is low at Cu contents of 0.6 wt.%, which may be because Cu affects the microstructure and oxide layer. Micro-galvanic corrosion in the microstructure will happen when the Cu content is high, speeding up the corrosion process[42,43].

At −0.9 V, the SCC sensitivity rates of 0.0Cu, 0.6Cu and 1.0Cu steel in the abiotic medium were 33.77%, 28.97% and 26.27%, while those in the biotic medium were 41.17%, 35.76% and 32.34%, respectively. The results show that the susceptibility of SCC decreases with the increase of Cu content

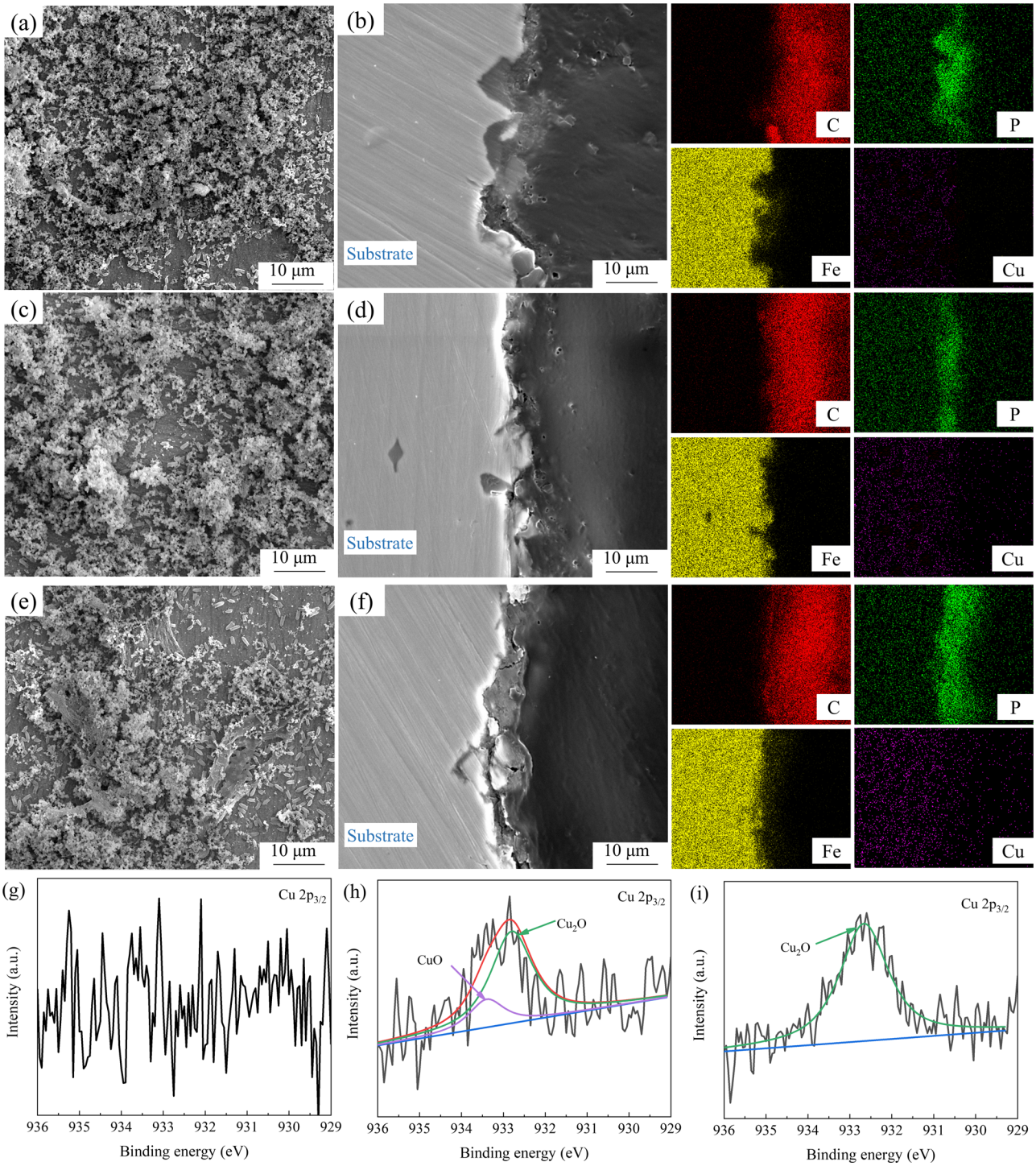

Fig. 6 | Surface, lateral morphology and composition analysis of different Cu-bearing steels after 7 days immersion in biotic medium. a, **b**, **g** 0.0Cu, **c**, **d**, **h** 0.6Cu, **e**, **f**, **i** 1.0Cu.

under cathodic polarization. Further analysis showed that the SCC sensitivity of *B. cereus* to different Cu-bearing steel was increased by 7.40%, 6.79% and 6.07%, which means that increasing Cu content can reduce the effect of *B. cereus* sensitivity to SCC. At the same time, it was found that, at −0.9 V, the decrease in SCC sensitivity after Cu addition was greater than that at the OCP, indicating that the negative shift of the cathode potential had a more obvious effect on SCC sensitivity. The optimal Cu content was 0.6 wt.% at OCP and 1.0 wt.% at cathode potential. The increase of Cu content can reduce the corrosion effect of *B. cereus* on steel and also effectively reduce the probability of SCC at cathodic potential. The SCC sensitivity is correlated with the effective hydrogen trap created by the Cu-rich phase because the cathode potential causes the galvanic corrosion in the microstructure to vanish.

Fracture analysis

Figure 11 shows the fracture morphologies of different Cu-bearing steel at OCP and −0.9 V in abiotic and biotic media. At the OCP, all fractures showed a certain degree of neck shrinkage. In the abiotic medium, dimpling existed at the initiation site of fracture (Fig. 11a, e, i), indicating that ductile fracture was the main feature, while in the biotic medium (Fig. 11b, f, j),

dimpling disappeared and the fracture mode was mainly quasi-cleavage, presenting a brittle fracture feature. The findings suggested that a *B. cereus* environment might cause a shift in fracture type from ductile to brittle.

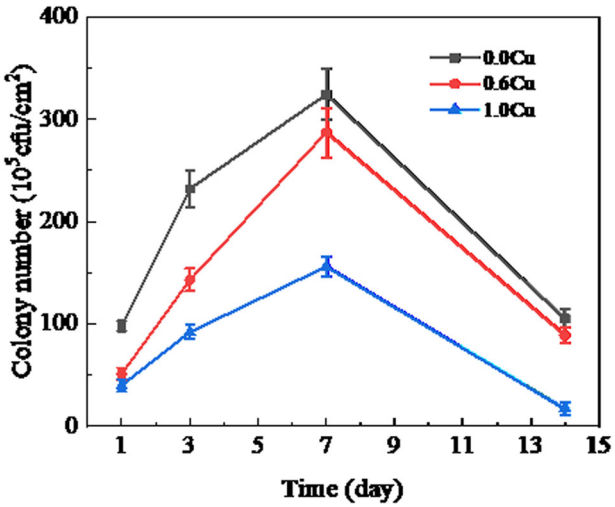

Fig. 7 | The variation of colony number. 0.0Cu, 0.6Cu and 1.0Cu steel surface after inoculation with initial planktonic cell concentration of 10^5 cells·mL^{-2} (mean ± standard deviation).

At −0.9 V (Fig. 11 c, g, k, d, h, l), all the fractures showed a low degree of neck shrinkage, no obvious dimples at the initial location of fracture, and the fracture morphology was fluvial pattern with the presence of tearing edges, showing brittle fracture characteristics. There was little difference in fracture morphology between abiotic and biotic media, demonstrating that under the influence of cathode potential, the effect of potential on material fracture is more noticeable than that of *B. cereus*.

Figure 12 shows the fracture profile morphologies of different Cu-containing steels at OCP and −0.9 V in abiotic and biotic media. All samples showed different degrees of uniform corrosion at the OCP. Further analysis of the crack morphology showed that the secondary crack width of 0.6Cu steel was smaller than that of the other two steels, showing a small degree of cracking characteristics, which was consistent with the results of SCC sensitivity. At the same time, the secondary crack morphology in abiotic and biotic media was compared respectively. The width and number of cracks in the biotic medium (Fig. 12b, f, j) were larger and more than those in the abiotic medium (Fig. 12a, e, i), indicating that *B. cereus* could promote the initiation and propagation of cracks. At −0.9 V, the corrosion morphology of the sample surface disappeared, indicating that the surface corrosion can be inhibited. With the increase of Cu content, the size of secondary cracks decreases, suggesting that the increase of Cu content can effectively reduce the initiation and propagation of cracks caused by cathode potential (trace hydrogen). Meanwhile, comparing the crack morphology in abiotic and biotic media, it was obviously found that the crack size in biotic medium was larger. Although Cu could effectively inhibit crack initiation and propagation, the role of *B. cereus* in promoting hydrogen penetration could not be ignored, which was consistent with the results of previous study[20].

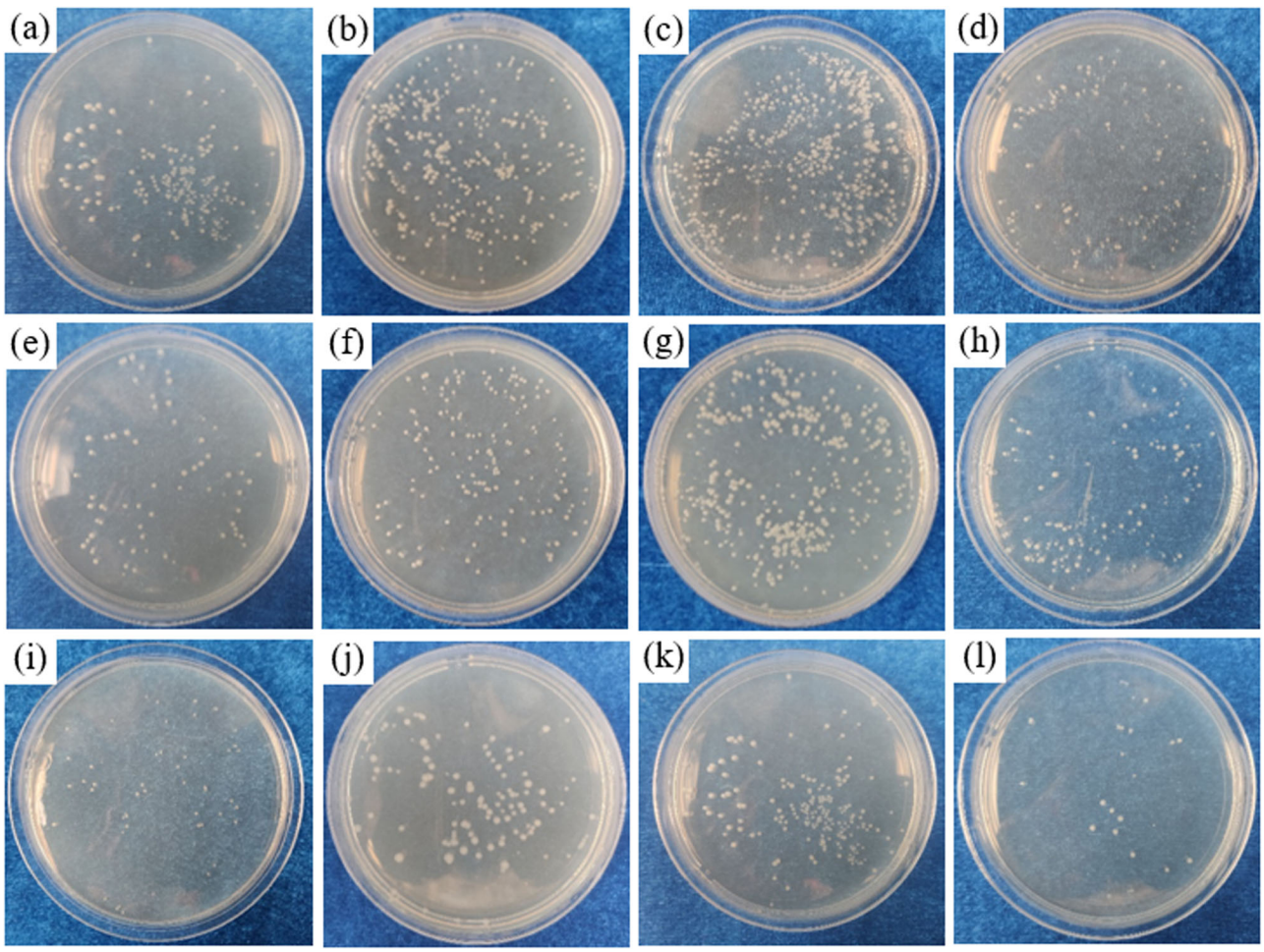

Fig. 8 | The colonies of *B. cereus* cultured from the biofilm samples collected from different Cu-bearing steels. a–d 0.0Cu, **e–h** 0.6Cu, **i–l** 1.0Cu, (**a**, **e**, **i**), (**b**, **f**, **j**), (**c**, **g**, **k**) and (**d**, **h**, **l**) are cultured 1, 3, 7 and 14 days respectively (10^5 cfu·cm^{-2}).

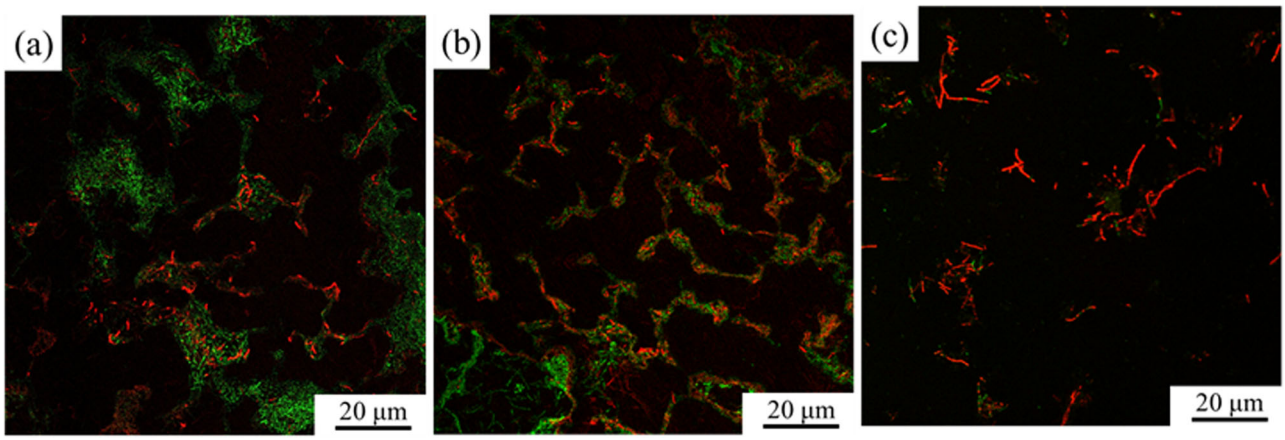

Fig. 9 | Live/dead staining of different Cu-bearing steel surfaces after 7 days of bacterial culture. a 0.0Cu, **b** 0.6Cu, **c** 1.0Cu.

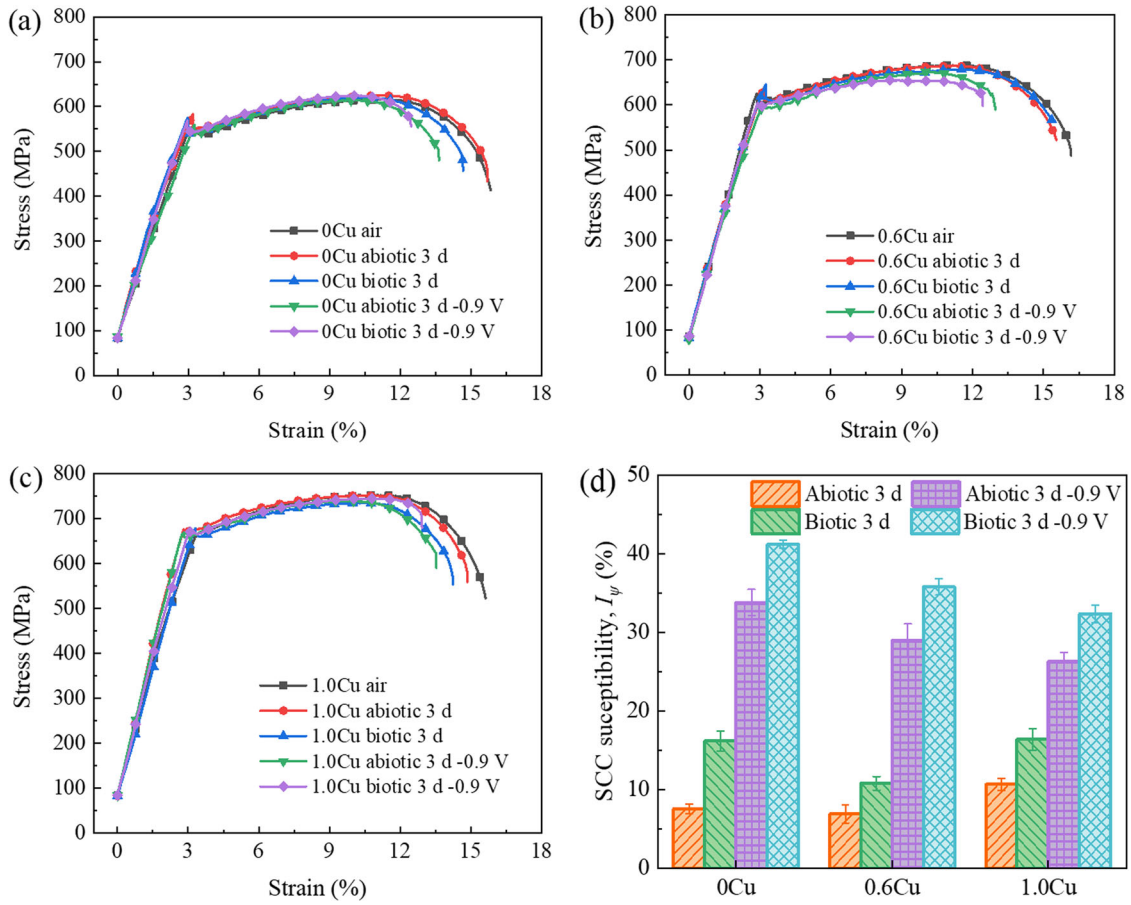

Fig. 10 | Stress-strain curves of different Cu-bearing steel in air, abiotic and biotic media. a 0.0Cu, **b** 0.6Cu, **c** 1.0Cu, **d** SCC susceptibility (Mean ± standard deviation).

To further observe the effect of *B. cereus* on crack propagation with different Cu contents at −0.9 V, the crack propagation morphology was observed, and the results are shown in Fig. 13. Different Cu contents have different crack propagation patterns. The crack width and depth of 0.0Cu, 0.6Cu and 1.0Cu steels decreased gradually, and the depths were 48.75 μm, 26.02 μm and 16.25 μm, respectively. There are some small crack branches in the main crack, indicating that the crack is mainly intergranular cracking, but at the same time, we can also see from the side that some cracks are transgranular cracking trend, so it indicates that this potential belongs to the transition stage from intergranular cracking to transgranular cracking. When the Cu content increased to 1.0 wt%, the crack depth decreased to 16.25 μm. No small crack branches were observed in the main crack, and the tip of the crack was sharp, indicating that the main crack was transgranular propagation. The change of fracture mode is mainly due to the difference of dislocation emission and interaction between dislocation and other defects in the steel, which changes the local atomic configuration near the crack path[44]. At −0.9 V, Cu can not only effectively reduce the crack propagation depth, but also change the fracture mode. This is because the precipitation of nano-sized Cu-rich phase in the Cu-bearing steel obtains a favorable trap for hydrogen capture, which makes the hydrogen entering the steel evenly distributed, and thus produces excellent hydrogen

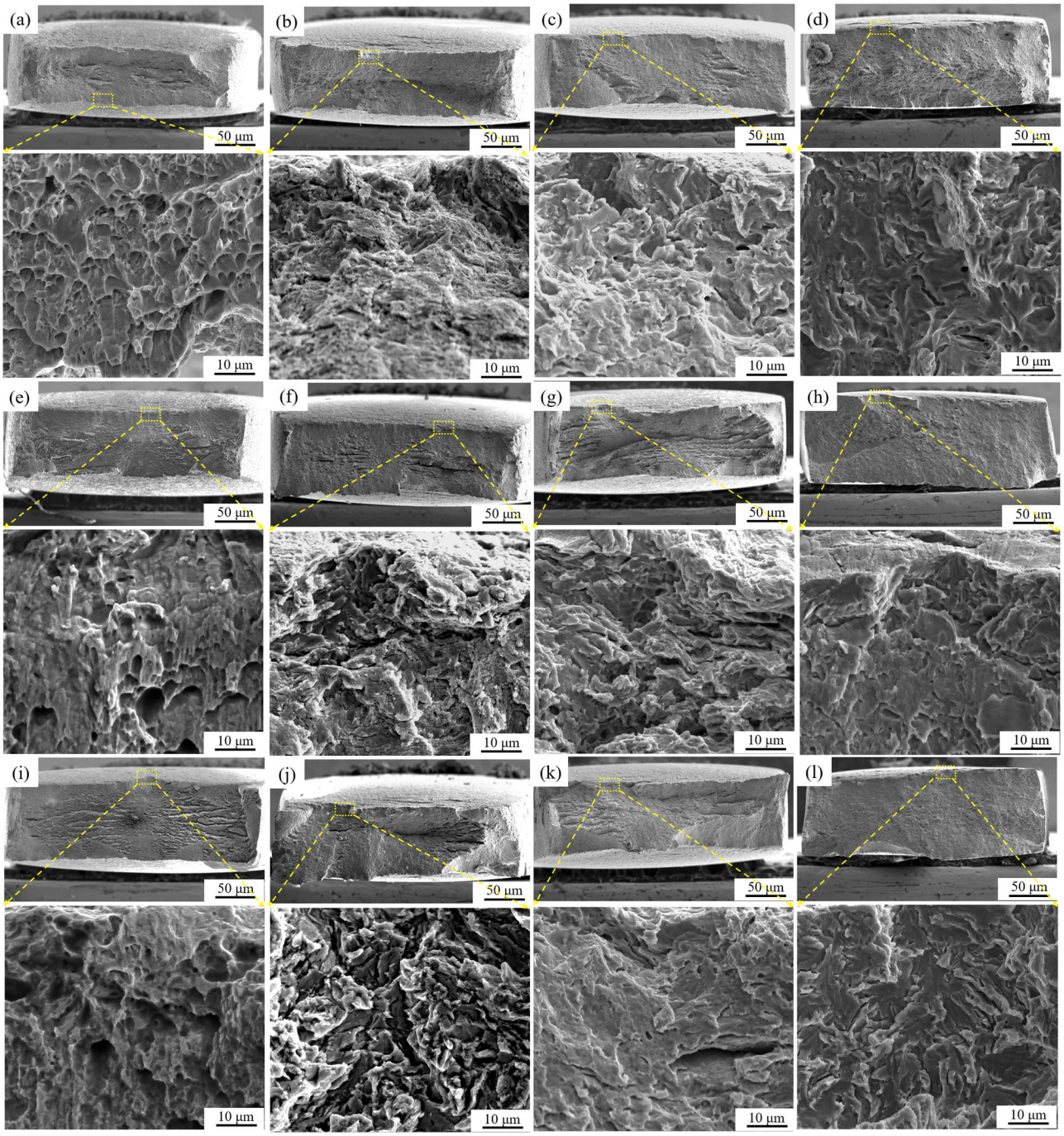

Fig. 11 | Fracture morphologies of different Cu-containing steels in different environments. a–d 0.0Cu, **e–h** 0.6Cu, **i–l** 1.0Cu, (**a**, **e**, **i**), (**b**, **f**, **j**), (**c**, **g**, **k**) and (**d**, **h**, **l**) are abiotic, biotic, abiotic @ −0.9 V, biotic @ −0.9 V, respectively.

cracking resistance to the Cu-bearing steel. Moreover, the addition of Cu in the process of SCC inhibits the dislocation movement, lowering the degree of local strain[45].

Resistance of Cu-bearing steel to *B. cereus* corrosion

It is commonly recognized that some metal elements, such as Cu, Zn, Co, and Mn, are needed for microorganisms. However, because there is little demand for these elements within cells, excess metals will bind to these substances instead of their typical sites, which can have hazardous effects[46,47]. Cu is the perfect element for creating antibacterial metal products because it is a cheap substance. In this study, the electrochemical tests revealed that the corrosion rate of the 1.0Cu steel is lower than that of the other two steels, suggesting that higher Cu content may have harmful effects on *B. cereus* and lessen their contribution to corrosion. The corrosion morphology also demonstrates that as the Cu concentration increases, the depth of the local corrosion reduces, suggesting that an increase in Cu content can to some extent prevent the corrosive action of *B. cereus*. Furthermore, the live/dead biofilm staining directly demonstrated that addition of Cu in the pipeline steel inhibited the bacteria growth and suppressed the formation of biofilm.

However, the antibacterial effect of Cu is a very complicated and multifactorial process. On the one hand, Cu exhibits its antibacterial property in several different forms. Ren et al. [48] analyzed Cu-bearing austenitic stainless steel of type 304, and they hypothesized that the antibacterial properties of the steel were caused by the precipitation of the ε-Cu phase. Akhavan[49] believed that CuO nanoparticles fixed by heat treatment of silica

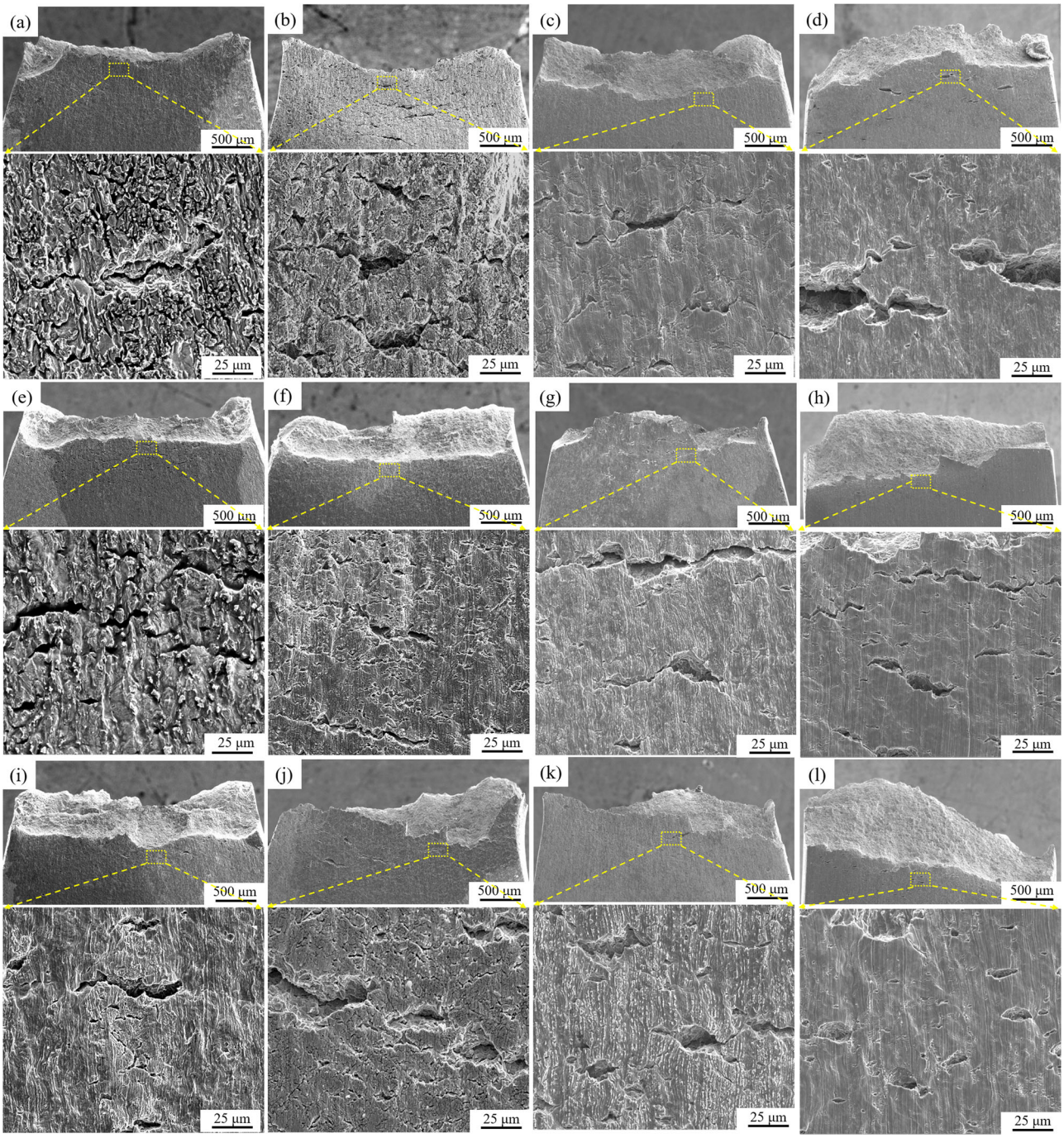

Fig. 12 | Lateral morphologies of different Cu-containing steels in different environments. a–d 0.0Cu, **e–h** 0.6Cu, **i–l** 1.0Cu, (**a**, **e**, **i**), (**b**, **f**, **j**), (**c**, **g**, **k**) and (**d**, **h**, **l**) are abiotic, biotic, abiotic @ −0.9 V, biotic @ −0.9 V, respectively.

thin film at 300 °C showed strong antibacterial activity against *Escherichia coli*. Xia et al. [28] suggested that the inhibition of biofilm was caused by the release of Cu ions from the Cu-rich phase in 2205-Cu duplex stainless steel, thus effectively alleviating the microbial corrosion of *P. aeruginosa*. The antibacterial action is mostly generated by the Cu ions released by the Cu-rich phase, according to Nan et al.[50], who also confirmed that the Cu-rich phase precipitation caused by Cu saturation in austenitic stainless steel is the essential factor in bacterial eradication. The key to the antibacterial activity was the nanometer-sized Cu-rich particles that precipitated from Cu-bearing steel after aging treatment in this study.

On the other hand, Cu exhibits its antibacterial property by several different antibacterial mechanisms. Cu acts as a catalyst to produce reactive oxygen species, which can cause oxidative damage to important cellular components such as proteins, nucleic acids and lipids[51]. Additionally, propensity of Cu to gain and lose electrons when switching between the oxidation states of Cu^{+} and Cu^{2+} is associated with its antibacterial activity[52]. The Cu-rich phase on the surface is also primarily oxidized by the environment at this time, and in the biofilm, typically through contact with bacteria, CuO can be reduced to metallic Cu, which inactivates the protein by destroying the cytoplasmic enzyme needed to produce branched amino acids[53].

Resistance of Cu-bearing steel to HE

Studying the impact of Cu reveals that it not only increases strength but also enhances resistance to HE[54]. In the SRB environment, Cu can promote the formation of a protective film of Cu and FeS_{1-x} on the

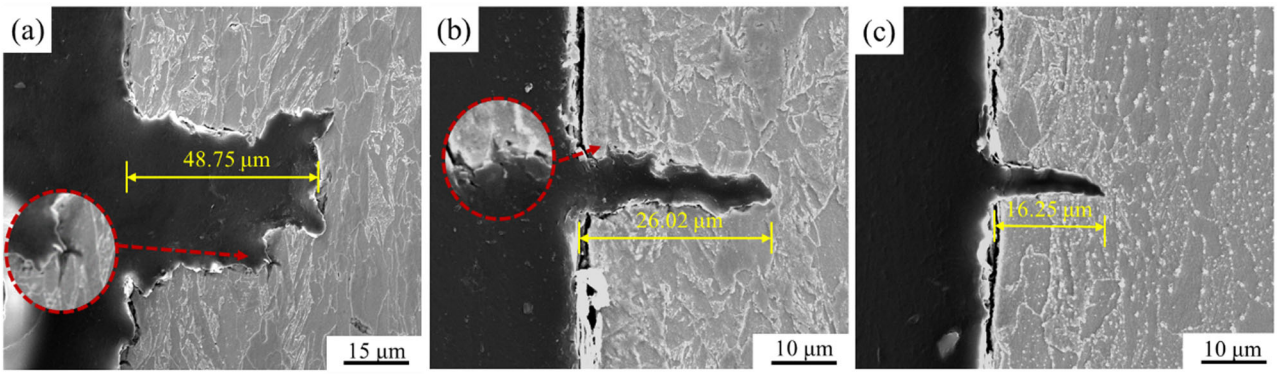

Fig. 13 | Crack propagation morphology of different Cu-containing steels in biotic medium at −0.9 V. a 0.0Cu, **b** 0.6Cu, **c** 1.0Cu.

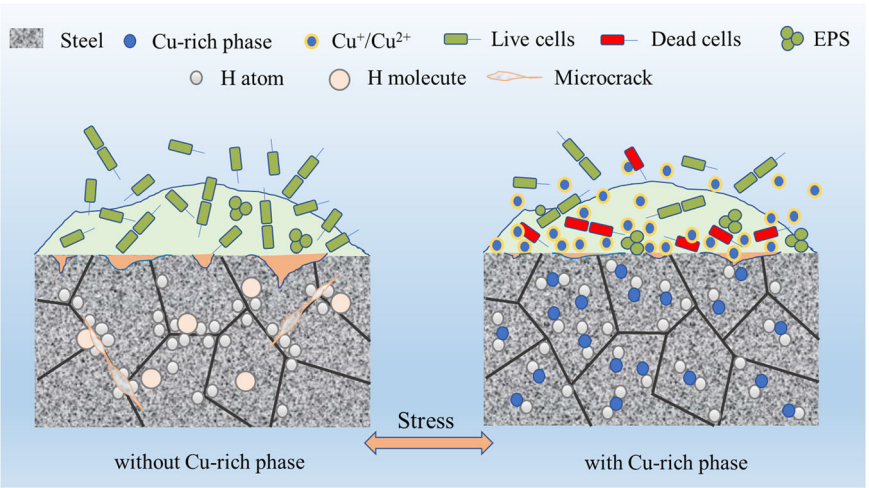

Fig. 14 | Schematic diagram of resistance mechanism of Cu-bearing steel to *B. cereus* and SCC. The steel without Cu precipitated phase is not only corroded by microorganisms, but also produces cracking, while the steel containing Cu precipitated phase causes bacterial death and disperses hydrogen accumulation.

steel surface, thereby minimizing the adsorption and penetration of hydrogen on the steel matrix[55]. According to this study, *B. cereus* have little effect on hydrogen adsorption in steel, and Cu has a greater effect on hydrogen in the microstructure. Trace Cu in typical pipeline steel has a minimal impact on hydrogen absorption, especially when the steel is overprotected by cathodic potential. Hydrogen atoms enter the steel and diffuse to the defect position between the lattice gaps, where they aggregate and combine to form gaseous molecules, causing rapid volume expansion and resulting cracks in this position[56]. Therefore, the key to preventing HE is to disperse the hydrogen into the steel as uniformly as possible rather than allowing it to aggregate.

Hydrogen trap is an efficient approach to be introduced by nano-precipitated phase in order to increase the resistance to HE. Takahashi[57] used Cu to reinforce and toughen pipeline steel in place of Mn. The findings demonstrated that the alloy grain was refined and the yield strength enhanced when the mass fraction of Cu was raised to 1.7 wt.%. Shi[58] added various Cu contents to X80 steel produced uniformly dispersed nano-Cu rich phases after aging at 500 °C for 1 h. These precipitated phases might contribute to hydrogen trapping as well as precipitation strengthening. In this study, hydrogen penetrates the steel matrix when the cathode potential is applied by SSRT, and the HE sensitivity is decreased by the Cu-rich phases scattered throughout the steel matrix, then the number of secondary cracks at the fracture area gradually decreased as the Cu content increased. This strongly suggested that the nano-Cu phase could function as a helpful hydrogen trap and effectively pin dislocation movement to prevent high HE in local areas.

Resistance of Cu-bearing steel to *B. cereus* and SCC

From the two aforementioned perspectives, the effects of Cu on the resistance to *B. cereus* and HE were illustrated separately. Since carbon steel is more likely than stainless steel to corrode in the environment, it releases more Cu ions, and the antibacterial effect is more significant. The main function of Cu resistance to *B. cereus* is to minimize the metabolism and the growth and adherence of biofilm on steel surfaces. Cathodic protection is typically utilized to safeguard subterranean pipelines in order to prevent corrosion. The protective effect will be impacted by either a shortage of protection potential or an overload of protection potential. The poisonous effect of Cu ions can reduce the impact of *B. cereus* when the protective potential is insufficient. The Cu-rich phase scattered in the microstructure can efficiently serve as a hydrogen trap to lessen the risk of HE when the protective potential is overwhelmed. As a result, adding the proper amount of Cu to pipeline steel has two effects on lowering *B. cereus* corrosion and SCC. Figure 14 illustrates the two mechanisms. The findings of this study not only widen the range of applications for the Cu-bearing pipeline steel that is resistant to MIC, but they also offer a fresh concept for creating steel materials with outstanding resistance to SCC.

In summary, the study herein revealed that the strength of steel increases as Cu content rises, although its elongation and impact toughness slightly decline and its antibacterial characteristic becomes more pronounced. Cu-rich phase plays a key role in releasing Cu ions to poison *B. cereus* after corrosion of the steel. Compared to 0.0 wt.% Cu steel, SCC sensitivity of 0.6 wt.% Cu steel increase is the lowest at OCP, reducing its increment from 8.61% to 3.89%, while 1.0 wt.% Cu steel SCC sensitivity increase is the smallest at −0.9 V, reduced from 7.40% to 6.07%. The nano Cu-rich phase can effectively operate as a hydrogen trap to lower the

Table 2 | Chemical compositions of experimental steels (wt.%)

Steel	C	Si	Mn	Cr	Mo	Ni	Cu	Nb	Fe
0.0Cu	0.06	0.15	1.29	0.29	0.29	0.71	0.02	0.13	Balance
0.6Cu	0.07	0.22	1.10	0.35	0.28	0.42	0.58	0.17	Balance
1.0Cu	0.06	0.20	1.35	0.26	0.29	0.29	1.01	0.13	Balance
2.0Cu	0.06	0.25	1.25	0.28	0.28	0.22	1.95	0.14	Balance

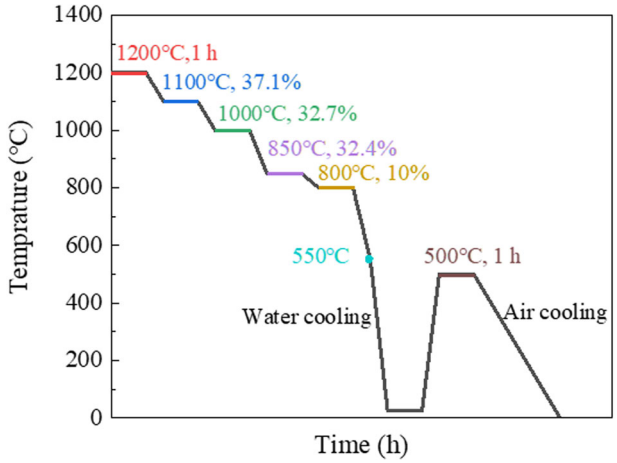

Fig. 15 | The schematic diagram of thermo-mechanical controlled processing (% meaning reduction amount). The relationship between temperature, reduction amount and time during controlled rolling and cooling of the material.

probability of HE, hence reducing the SCC sensitivity of *B. cereus* to pipeline steel.

Methods

Materials and characterization

The welding performance of pipeline steel is fully taken into account in the composition design of pipeline steel with varying Cu contents. According to an acceptable carbon equivalent formula, the final composition test results for medium/high strength non-quenched and tempered low-alloy steel (500–900 MPa) are as indicated in Table 2. Four different types of billets were heat treated using controlled rolling and controlled cooling technologies to produce ferrite, pearlite, or bainite microstructures. The billets were austenitized at 1180–1200 °C for 1 h, and then rolled 5 times under regulated temperatures for 5–10 s each time, until it reached its final thickness of 10 mm. After rolling, it was cooled with water to room temperature. To get the material used in this study, the rolled plate is aged at 500 °C for 1 h and then air-cooled to room temperature. The schematic diagram of thermo-mechanical controlled processing is shown in Fig. 15.

A shock test apparatus (ZBC2000, SANS, USA) was used to evaluate the low-temperature impact resistance of four distinct experimental steels. The sample size, surface treatment, and testing procedure all adhere to the standard (GB/T229-2020). Microstructures of experimental steels were observed using scanning electron microscopy (SEM, Quanta 250, USA) and transmission electron microscope (TEM, Tecnai G20, USA). For the SEM observation, samples were mechanically ground to 2000# with sand papers, polished, and then etched in a 2% nital solution. For the TEM observation, 50-μm thin disks were obtained after electro-polished by a twin-jet electropolisher in a solution of 10 vol.% perchloric acid and 90 vol.% ethanol. The morphology and composition analysis of the microstructures were examined by a TEM at an accelerating voltage of 200 kV.

Bacterium and medium

Bacillus cereus (B. cereus), a typical NRB, was isolated from the surrounding soil of an X80 pipeline steel specimen (100 mm × 75 mm × 5 mm) that had been buried for two years in Beijing soil (NL 39°79, EL 116°35, average temperature 12.9 °C, moisture 14.38, salinity 0.198%, pH 6.96). Evolutionary trees and their nitrate reducibility were analyzed as described in our previous study[59]. The composition of the near-neutral pH solution was ($g{\cdot}L^{-1}$): 0.5 yeast extract, 1 tryptone, 1 NaCl, 1 $NaNO_3$, 0.483 $NaHCO_3$, 0.122 KCl, 0.137 $CaCl_2$, and 0.131 $MgSO_4{\cdot}7H_2O$. The medium was sterilized at 121 °C for 20 min prior to the experiment, and it was then chilled for 2 h while being continuously pumped with 5% CO_2 balanced with N_2 to achieve an anaerobic and near-neutral pH condition, which simulated the environment formed after coating disbonding in the buried pipeline[60,61]. Bacterial seeds were cultivated in the aforementioned solution at 30 °C for 24 h at a ratio of 1:100 (v:v) for the biotic medium. To ensure that the entire experimental procedure was uncontaminated, no bacteria were added to the culture media for the abiotic medium. Unless otherwise stated, all tests were sealed and carried out at 30 °C without oxygen.

Corrosion test

Electrochemical tests were performed in a typical three-electrode system. The working electrode (WE) was connected by copper wire with an exposed area of 1 cm^2. A platinum sheet and saturated calomel electrode (SCE) were used as the counter and reference electrodes (RE), respectively. The electrochemical tests were performed through a workstation (Gamry, Reference 600+, USA) using a typical three-electrode system. The bacteria were inoculated at the beginning of the experiment, electrochemical impedance spectroscopy (EIS) was performed for 1, 3, 7, and 14 days at a sinusoidal voltage signal of 10 mV in the frequency range of 10^{-2}–10^4 Hz. The EIS data were analyzed using the Zsimpwin software (Scribner) and Echem Analyst (Gamry), respectively. The samples were retrieved carefully after being submerged in biotic medium for 7 days, and they were then shifted to a 2.5% glutaraldehyde solution for 8 hours at 4 °C in a refrigerator. The samples were then treated with ethanol in concentrations of 50%, 60%, 70%, 80%, 90%, and 100% (v:v) for 8 minutes before drying naturally. The surface morphology and cross-section morphology were observed via SEM with a beam voltage of 25 kV. The corrosion product elements were analyzed via X-ray photoelectron spectroscopy (XPS, Smartlab 9 kW, JPN).

Antibacterial efficacy assay

Different samples were put in 24-well plates, and the same concentration of *B. cereus* were injected and incubated for 1, 3, 7, and 14 days, respectively. Sessile bacteria were discharged through a vortex after planktonic cells were eliminated using phosphate buffer saline (PBS). To count the number of colonies, a series of diluted bacterial suspensions were put on agar plates and grown at 37 °C for 12–24 h. Live/dead staining is performed after 7 days of immersion. After the samples were rinsed with PBS, 1 mL PBS, 25 μL SYTO-9 dye and PI dye were added in a darkroom and left for 20 min. The biofilm was then observed under a confocal laser scanning microscopy (CLSM, Leica TCS SP8, GER), where the SYTO-9 dye showed green fluorescence at 488 nm excitation wavelength to detect living cells and the PI showed red fluorescence at 559 nm excitation wavelength to stain dead cells.

SSRT

The size of tensile specimens and experimental device are shown in Fig. 16. Following aseptic preparation, the test box containing the tensile specimen, CE, and RE was filled with the inoculated solution before being sealed. Previous studies[20] have shown the *B. cereus* system to have the maximum effect on the SCC sensitivity of X80 steel at −0.9 V (SCE), which was attributed to the possibility of affecting both the physiological activities of *B. cereus* and hydrogen embrittlement. Therefore, the cathode potential is applied at the beginning of the experiment, and the same parameters were used in this experiment to investigate the SCC sensitivity of different Cu-bearing steels.

The SSRT was carried out under the tensile testing machine (Letry, WDML-30 kN, CHN). After 3 days of potential application and bacterial culture, the sample was preloaded 1000 N to eliminate the crevice inside the machine and fixture gap, and then proceeded at a tensile rate of

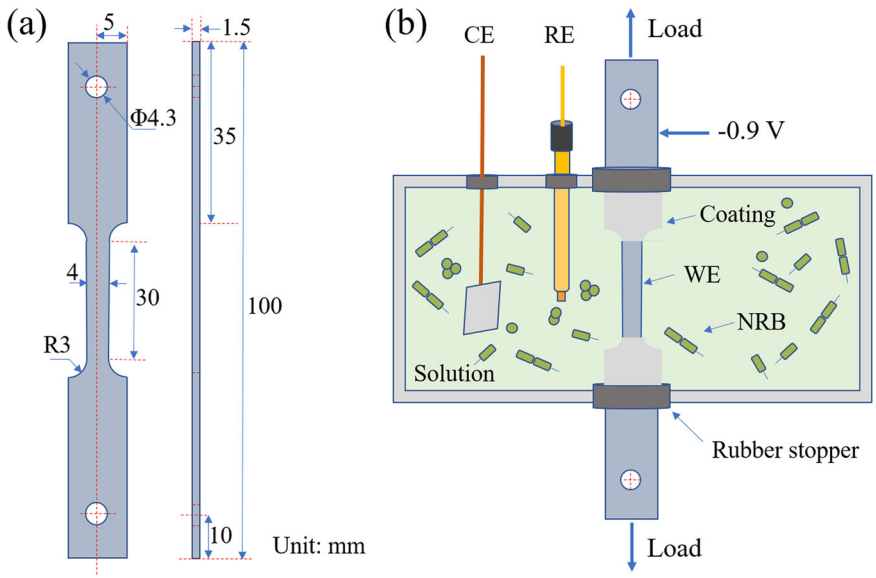

Fig. 16 | Schematic diagram of the SSRT samples and solution cell. a Detailed dimensions of sample, **b** schematic diagram of the solution cell for SSRT.

$1 \times 10^{-6}\,s^{-1}$ after stabilization. The decrease in the reduction of area (I_ψ) was calculated using the following equation to evaluate the SCC susceptibility:

$$I_\Psi = \left(1 - \frac{\Psi_s}{\Psi_0}\right) \times 100\% \quad (1)$$

where Ψ_s and Ψ_0 are the percentage reductions of area in the medium and air, respectively. After the fracture specimens were sliced to remove the surplus part. the fracture and lateral surfaces of the specimens were studied using SEM after the corrosion products were cleaned with a derusting solution (3.5 g hexamethylenetetramine was added to 500 mL hydrochloric acid and 500 mL deionized water).

Data availability

All data generated or analyzed during this study are included in this published article and any additional data that support the findings of this study are available from the corresponding author upon reasonable request.

Received: 15 November 2023; Accepted: 15 March 2024;
Published online: 06 April 2024

References

1. Xu, D., Gu, T. & Lovley, D. R. Microbially mediated metal corrosion. *Nat. Rev. Microbiol.* **21**, 705–718 (2023).
2. Cámara, M. et al. Economic significance of biofilms: a multidisciplinary and cross-sectoral challenge. *NPJ Biofilms Micro.* **8**, 42 (2022).
3. Gu, T. Y., Wang, D., Lekbach, Y. & Xu, D. Extracellular electron transfer in microbial biocorrosion. *Curr. Opin. Electroche.* **29**, 100763 (2021).
4. Xu, D. K., Li, Y. C. & Gu, T. Y. Mechanistic modeling of biocorrosion caused by biofilms of sulfate reducing bacteria and acid producing bacteria. *Bioelectrochemistry* **110**, 52–58 (2016).
5. Keresztes, Z., Felhősi, I. & Kálmán, E. Role of redox properties of biofilms in corrosion processes, Electrochim. *Acta* **46**, 3841–3849 (2001).
6. Sowards, J. W. & Mansfield, E. Corrosion of copper and steel alloys in a simulated underground storage-tank sump environment containing acid-producing bacteria. *Corros. Sci.* **87**, 460–471 (2014).
7. Spark, A., Wang, K., Cole, I., Law, D. & Ward, L. Microbiologically influenced corrosion: a review of the studies conducted on buried pipelines. *Corros. Rev.* **38**, 231–262 (2020).
8. Little, B. J., Hinks, J. & Blackwood, D. J. Microbially influenced corrosion: Towards an interdisciplinary perspective on mechanisms. *Int. Biodeterior. Biodegrad.* **154**, 105062 (2020).
9. Al-Nabulsi, K. M., Al-Abbas, F. M., Rizk, T. Y. & Salameh, A. A. E. M. Microbiologically assisted stress corrosion cracking in the presence of nitrate reducing bacteria. *Eng. Fail. Anal.* **58**, 165–172 (2015).
10. Liu, B. et al. Stress corrosion cracking of X80 steel heat-affected zone in a near-neutral pH solution containing Bacillus cereus. *Npj. Mat. Degrad.* **7**, 27 (2023).
11. Wu, T. Q. et al. Stress corrosion cracking of X80 steel in the presence of sulfate-reducing bacteria. *J. Mater. Sci. Technol.* **31**, 413–422 (2015).
12. Javaherdashti, R., Raman, R., Panter, C. & Pereloma, E. Microbiologically assisted stress corrosion cracking of carbon steel in mixed and pure cultures of sulfate reducing bacteria. *Int. Biodeterior. Biodegrad.* **58**, 27–35 (2006).
13. Sun, D. X., Wu, M. & Xie, F. Effect of sulfate-reducing bacteria and cathodic potential on stress corrosion cracking of X70 steel in sea-mud simulated solution. *Mater. Sci. Eng. A* **721**, 135–144 (2018).
14. Xie, F. et al. Stress corrosion cracking behavior induced by Sulfate-reducing bacteria and cathodic protection on X80 pipeline steel. *Constr. Build. Mater.* **308**, 125093 (2021).
15. Xu, D. K., Li, Y. C., Song, F. M. & Gu, T. Laboratory investigation of microbiologically influenced corrosion of C1018 carbon steel by nitrate reducing bacterium Bacillus licheniformis. *Corros. Sci.* **77**, 385–390 (2013).
16. Wei, B., Xu, J., Sun, C. & Cheng, Y. F. Internal microbiologically influenced corrosion of natural gas pipelines: A critical review. *J. Nat. Gas. Sci. Eng.* **102**, 104581 (2022).
17. Miller, R. B., Lawson, K., Sadek, A., Monty, C. N. & Senko, J. M. Uniform and Pitting Corrosion of Carbon Steel by Shewanella oneidensis MR-1 under Nitrate-Reducing Conditions. *Appl. Environ. Microbiol.* **84**, e00790–00718 (2018).
18. Liu, B. et al. Corrosion mechanism of nitrate reducing bacteria on X80 steel correlated to its intermediate metabolite nitrite. *Constr. Build. Mater.* **303**, 124454 (2021).
19. Lu, S. et al. Extracellular electron transfer corrosion mechanism of two marine structural steels caused by nitrate reducing Halomonas titanicae. *Corros. Sci.* **217**, 111125 (2023).
20. Liu, B., Liu, M., Liu, Z., Du, C. & Li, X. Nitrate-reducing-bacteria assisted hydrogen embrittlement of X80 steel in a near-neutral pH solution. *Corros. Sci.* **202**, 110317 (2022).

21. Fu, Q. et al. Mechanistic diversity between nitrate and nitrite on biocorrosion of X80 pipeline steel caused by Desulfovibrio desulfuricans and Pseudomonas stutzeri. *Corros. Sci.* **207**, 110573 (2022).
22. Wan, H., Song, D., Du, C., Liu, Z. & Li, X. Effect of alternating current and Bacillus cereus on the stress corrosion behavior and mechanism of X80 steel in a Beijing soil solution. *Bioelectrochemistry* **127**, 49–58 (2019).
23. Royani, A., Hanafi, M., Julistiono, H. & Manaf, A. The total phenolic and flavonoid contents of Aloe vera and Morinda citrifolia extracts as antibacterial material against Pseudomonas aeruginosa. *Mat. Today Phys.* **72**, 2796–2802 (2023).
24. Lou, Y. et al. Antibacterial ability of a novel Cu-bearing 2205 duplex stainless steel against Pseudomonas aeruginosa biofilm in artificial seawater. *Int. Biodeterior. Biodegrad.* **110**, 199–205 (2016).
25. Liang, Y. et al. Effect of electroless plating time and temperature on the formation and antibacterial ability of Cu-plated cement-based material. *Cem. Concr. Compos.* **131**, 104566 (2022).
26. Yuan, Y. et al. Design of a new Ti-Mo-Cu alloy with excellent mechanical and antibacterial properties as implant materials. *Mater. Lett.* **306**, 130875 (2022).
27. Thurman, R. B., Gerba, C. P. & Bitton, G. The molecular mechanisms of copper and silver ion disinfection of bacteria and viruses. *Crit. Rev. Environ. Control* **18**, 295–315 (1989).
28. Xia, J. et al. Laboratory investigation of the microbiologically influenced corrosion (MIC) resistance of a novel Cu-bearing 2205 duplex stainless steel in the presence of an aerobic marine Pseudomonas aeruginosa biofilm. *Biofouling* **31**, 481–492 (2015).
29. Jiang, J. et al. Effects of aging time on intergranular and pitting corrosion behavior of Cu-bearing 304L stainless steel in comparison with 304L stainless steel. *Corros. Sci.* **113**, 46–56 (2016).
30. Zhao, J. et al. Effect of anodic polarization treatment on microbiologically influenced corrosion resistance of Cu-bearing stainless steel against marine Pseudomonas aeruginosa. *Corros. Sci.* **207**, 110592 (2022).
31. Xu, D. et al. Enhanced resistance of 2205 Cu-bearing duplex stainless steel towards microbiologically influenced corrosion by marine aerobic Pseudomonas aeruginosa biofilms. *J. Mater. Sci. Technol.* **34**, 1325–1336 (2018).
32. Ren, G. Y. et al. Enhanced antibacterial behavior of a novel Cu-bearing high-entropy alloy. *J. Mater. Sci. Technol.* **117**, 158–166 (2022).
33. Zhou, E. et al. A novel Cu-bearing high-entropy alloy with significant antibacterial behavior against corrosive marine biofilms. *J. Mater. Sci. Technol.* **46**, 201–210 (2020).
34. Wu, P. et al. Integrative chemical and omics analyses reveal copper biosorption and tolerance mechanisms of Bacillus cereus strain T6. *J. Hazard. Mater.* **435**, 129002 (2022).
35. Kong, J., Zhang, S., Shen, M., Zhang, J. & Yoganathan, S. Evaluation of copper(I)-doped zinc oxide composite nanoparticles on both gram-negative and gram-positive bacteria. *Colloids Surf. Physicochem. Eng. Asp.* **643**, 128742 (2022).
36. Xi, X. et al. The role of reverted transformation in hydrogen embrittlement of a Cu-containing low carbon high strength steel. *J. Mater. Res. Technol.* **25**, 5990–5999 (2023).
37. Yoo, J. et al. Effects of Cu addition on resistance to hydrogen embrittlement in 1 GPa-grade duplex lightweight steels. *Acta Mater.* **196**, 370–383 (2020).
38. Sun, H. et al. Optimizing the hydrogen embrittlement resistance by tuning the structures of Cu-rich nanoprecipitates in high strength martensite stainless steels. *Acta Mater.* **246**, 118722 (2023).
39. Wang, J. et al. Response of hydrogen diffusion and hydrogen embrittlement to Cu addition in low carbon low alloy steel. *Mater. Charact.* **195**, 112478 (2023).
40. Schutz, P. et al. Onto the role of copper precipitates and reverted austenite on hydrogen embrittlement in 17-4 PH stainless steel. *Mater. Charact.* **202**, 113044 (2023).
41. Dong, F. et al. Enhancement of hydrogen embrittlement resistance in a Fe-18Mn-0.6C twinning induced plasticity steel by copper alloying. *Acta Mater.* **254**, 118888 (2023).
42. Morcillo, M., Díaz, I., Chico, B., Cano, H. & de la Fuente, D. Weathering steels: From empirical development to scientific design. A review. *Corros. Sci.* **83**, 6–31 (2014).
43. Li, Z. et al. Role of segregation behavior of Cu and Sb in the region of inclusions on initial corrosion. *Npj. Mat. Degrad.* **7**, 29 (2023).
44. Pei, Z. et al. Towards understanding and prediction of atmospheric corrosion of an Fe/Cu corrosion sensor via machine learning. *Corros. Sci.* **170**, 108697 (2020).
45. Yang, H. et al. Nanoprecipitates induced dislocation pinning and multiplication strategy for designing high strength, plasticity and conductivity Cu alloys. *Scr. Mater.* **195**, 113741 (2021).
46. Bisht, N. et al. Recent advances in copper and copper-derived materials for antimicrobial resistance and infection control. *Curr. Opin. Biomed. Eng.* **24**, 100408 (2022).
47. Liu, J. et al. Transcription profiling-guided remodeling of sulfur metabolism in synthetic bacteria for efficiently capturing heavy metals. *J. Hazard. Mater.* **403**, 123638 (2021).
48. Ren, L., Nan, L. & Yang, K. Study of copper precipitation behavior in a Cu-bearing austenitic antibacterial stainless steel. *Mater. Des.* **32**, 2374–2379 (2011).
49. Akhavan, O. & Ghaderi, E. Cu and CuO nanoparticles immobilized by silica thin films as antibacterial materials and photocatalysts. *Surf. Coat. Technol.* **205**, 219–223 (2010).
50. Nan, L., Cheng, J. L. & Yang, K. Antibacterial behavior of a Cu-bearing type 200 stainless steel. *J. Mater. Sci. Technol.* **28**, 1067–1070 (2012).
51. Santo, C. E. et al. Bacterial killing by dry metallic copper surfaces. *Appl. Environ. Microbiol.* **77**, 794–802 (2011).
52. O'Gorman, J. & Humphreys, H. Application of copper to prevent and control infection. Where are we now? *J. Hosp. Infect.* **81**, 217–223 (2012).
53. Burla, A., Khandelwal, M. & Vaidya, M. Antibacterial properties of Cu containing complex concentrated alloys. *Mater. Today Commun.* **33**, 104915 (2022).
54. Song, H., Jo, M. & Kim, D. W. Vanadium or copper alloyed duplex lightweight steelwith enhanced hydrogen embrittlement resistance at room temperature. *Mater. Sci. Eng. A* **817**, 141347 (2021).
55. Xie, C. et al. The dependence of anti-corrosion behaviors of iron sulfide films on different reactants. *Int. J. Hydrog. Energy* **45**, 17548–17556 (2020).
56. Kwon, Y. J., Lee, T., Lee, J., Chun, Y. S. & Lee, C. S. Role of Cu on hydrogen embrittlement behavior in Fe–Mn–C–Cu TWIP steel,. *Int. J. Hydrog. Energy* **40**, 7409–7419 (2015).
57. Takahashi, A. & Iino, M. Microstructural refinement by Cu addition and Its effect on strengthening and toughening of sour service line pipe steels. *ISIJ Int.* **36**, 241–245 (1996).
58. Shi, X. B., Yan, W., Wang, W., Shan, Y. & Yang, K. Novel Cu-bearing high-strength pipeline steels with excellent resistance to hydrogen-induced cracking. *Mater. Des.* **92**, 300–305 (2016).
59. Liu, B., Li, Z. Y., Yang, X. J., Du, C. & Li, X. Microbiologically influenced corrosion of X80 pipeline steel by nitrate reducing bacteria in artificial Beijing soil. *Bioelectrochemistry* **135**, 107551 (2020).
60. Liu, Z. Y., Li, X. G. & Cheng, Y. F. Mechanistic aspect of near-neutral pH stress corrosion cracking of pipelines under cathodic polarization. *Corros. Sci.* **55**, 54–60 (2012).
61. Abedi, S. S., Abdolmaleki, A. & Adibi, N. Failure analysis of SCC and SRB induced cracking of a transmission oil products pipeline. *Eng. Fail. Anal.* **14**, 250–261 (2007).

Acknowledgements
This work was supported by Natural Science Basic Research Program of Shaanxi (No. 2024JC-YBQN-0457), and the National Natural Science Foundation of China (No. 51871026]).

Author contributions
Bo Liu conducted the experimental work under the supervision of Cuiwei Du, Fangyuan Lu evaluated and visualized the results, and Shidong Zhu drafted, reviewed and edited the paper. Xiaogang Li provided funding support.

Competing interests
The authors declare no competing interests.

Additional information
Correspondence and requests for materials should be addressed to Cuiwei Du.